Pattern Dimensions and Feature Shapes of Ternary Blends of Block Copolymer and Low Molecular Weight Homopolymers Directed To Assemble on Chemically Nanopatterned Surfaces

Umang Nagpal,[†] Huiman Kang,[†] Gordon S. W. Craig, Paul F. Nealey,[*] and Juan J. de Pablo

Department of Chemical and Biological Engineering, University of Wisconsin—Madison, 1415 Engineering Drive, Madison, Wisconsin 53706, United States. [†]These authors contributed equally to the work.

ABSTRACT Ternary blends of cylinder-forming polystyrene-*block*-poly(methyl methacrylate) (PS-*b*-PMMA) and low molecular weight PS and PMMA were directed to assemble on chemically patterned surfaces with hexagonal symmetry. The chemical patterns consisted of strongly PMMA preferential spots, patterned by electron-beam lithography, in a matrix of PS. The spot-to-spot spacing of the chemical patterns (L_s) was varied between $0.9L_0$ and $1.1L_0$, where L_0 is the cylinder-to-cylinder spacing of the pure block copolymer in bulk. The homopolymer volume fraction of the blends (ϕ_H) was varied between 0 and 0.3. In addition, chemical patterns were formed with selected spots missing from the perfect hexagonal array, such that the interpolation of domains between patterned spots could be examined on patterns where the polymer/pattern feature density ranged from 1:1 to 4:1. The assemblies were analyzed with top-down SEM, from which orientational order parameter (OP_o) values were determined. The SEM analysis was complemented by Monte Carlo simulations, which offered insights into the shapes of the assembled cylindrical domains. It was found that, in comparison to pure block copolymer, adding homopolymer increased the range of L_s values over which assemblies with high OP_o values could be achieved for 1:1 assemblies. However, the corresponding simulations showed that in the 1:1 assemblies the shape of the cylinders was more uniform for pure block copolymer than for blends. In the case of the 4:1 assemblies, the range of L_s values over which assemblies with high OP_o values could be achieved was the same for all values of ϕ_H tested, but the domains of the pure block copolymer had a more uniform shape. Overall, the results provided insights into the blend composition to be used to meet technological requirements for directed assembly with density multiplication.

KEYWORDS: block copolymer · ternary blend · thin film · chemical pattern · density multiplication · commensurability · bit patterned media · blends

Directed assembly of cylinder-forming block copolymer thin films has been used to form structures that have the potential as lithographic templates to enhance technologies ranging from semiconductors to bit patterned media.[1−10] Cylindrical domains that align perpendicularly to the substrate can be obtained by directed assembly of block copolymers on lithographically defined chemical patterns. If the geometry and chemistry of the chemical pattern are judiciously chosen, the underlying pattern can be used to create block copolymer films that have useful, well-defined nanostructures with both registration and a high degree of perfection and are suitable for pattern transfer from the block copolymer film into the substrate.[11−13] Additionally, directing the assembly of the cylindrical domains on chemically nanopatterned surfaces has been shown to be a viable method for decreasing the variation in critical dimensions while enhancing resolution and maintaining the uniformity of the three-dimensional shape of the patterned nanostructures.[14,15]

To meet the manufacturing constraints in many applications, block copolymer materials often must be able to fabricate various pattern geometries at once. As an example, many research groups have tried to apply directed assembly to the fabrication of bit patterned media.[16−19] From a manufacturing standpoint, one of the important constraints of bit patterned media is that the bits must be arranged in concentric rings within annular zones on the disk.[20] To maintain constant read-out frequency within a single zone at a constant angular velocity, the spacing of bits must vary from ring to ring within each zone. The bits on the inner rings within a zone will necessarily have to be closer together than the bits on the outer rings in the zone. Typically, the width of the annular zones requires a change in spacing of the bits from ring to ring of 5% or more. Therefore, the block copolymers that will be assembled on chemical patterns should have the flexibility to control the distance between the cylindrical domains.

* Address correspondence to nealey@engr.wisc.edu.

Received for review April 11, 2011 and accepted June 10, 2011.

Published online June 10, 2011
10.1021/nn201335v

© 2011 American Chemical Society

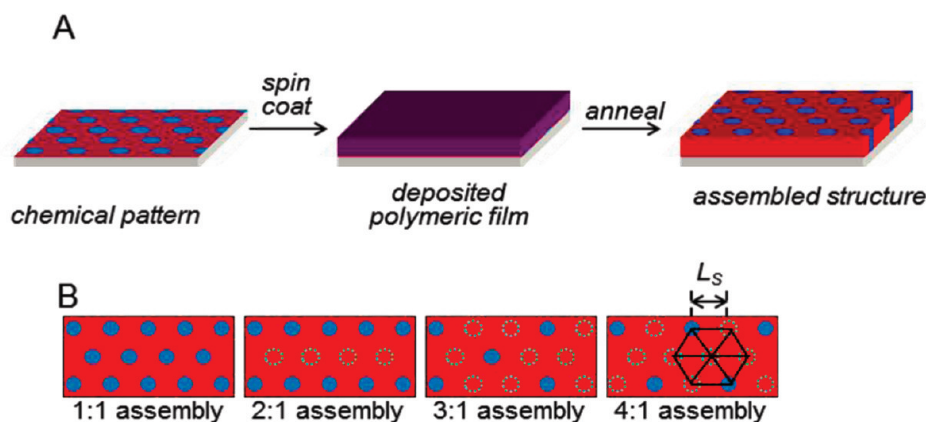

Figure 1. (A) Schematic of directed assembly of polymeric materials (either pure PS-*b*-PMMA or PS-*b*-PMMA/PS/PMMA ternary blends) on a chemical pattern. (B) Diagrams of chemical patterns designed for density multiplication factors ranging from 1:1 to 4:1, with the center-to-center spacing of spots on the pattern shown for the 1:1 and 4:1 cases. The solid blue spots represent patterned and etched spots in the chemical pattern, and the dashed circles represent the expected locations of assembled domains above the chemical pattern.

The challenge with directing the assembly of block copolymers with chemical patterns that have a range of values of pattern spacing periods (L_s) is that directed assembly typically works best when L_s is commensurate with the natural bulk period of the block copolymer, L_0.[21,22] In essence, the assembled block copolymer would need to be able to adjust to mismatches between L_s and L_0. Research has shown that, in the case of lamellae-forming block copolymers, directed assembly yields well-ordered structures when L_s differs from L_0 by as much as 10%.[23] In the case of cylinder-forming block copolymers, which can provide a spot pattern appropriate for bit patterned media, directed assembly can yield good structures when the incommensurability between L_s and L_0 is ∼5% or less and is nonsymmetric around L_0.[24] It would be technologically beneficial if the range of incommensurability over which directed assembly of cylindrical domains yields well-ordered structures could be increased.

In this work, we investigate using blends of low molecular weight (M_n) homopolymers and a cylinder-forming block copolymer to accommodate incommensurate values of L_s (with respect to L_0) in directed assembly, both with and without density multiplication. We examine assemblies with density multiplication factors ranging from 1:1 to 4:1, with blend homopolymer volume fractions (ϕ_H) ranging from 0 to 0.3, and L_s values ranging from $0.9L_0$ to $1.1L_0$. For our materials, we use polystyrene-*block*-poly(methyl methacrylate) (PS-*b*-PMMA) combined with low M_n PS and PMMA homopolymers to form ternary blends, similar to a subset of cylinder-forming blends studied by Stuen *et al.*[25] We use scanning electron microscopy (SEM) to image the assembled structures and characterize the order of the structures by calculating their orientational order parameter (OP_o).[26] We also use Monte Carlo simulations to gain insight into the three-dimensional structure of the assembled domains within the film, as well as location of the block copolymer and the homopolymer within the film.[27]

RESULTS

Directed Assembly of Ternary Blends without Density Multiplication. The general approach for directing the assembly of thin films of PS-*b*-PMMA or PS-*b*-PMMA/PS/PMMA ternary blends is shown in Figure 1A. We first examined the combined effects of ϕ_H of the ternary blends and the commensurability of L_s with L_0 on the assembly of thin films of PS-*b*-PMMA or PS-*b*-PMMA/PS/PMMA ternary blends on chemical patterns without density multiplication, such that the number of patterned spots on the substrate was equal to the number of cylinders to be assembled above the pattern. Figure 2 presents an array of top-down SEMs of the assembled films, with ϕ_H ranging from 0 to 0.3 and L_s ranging from $0.90L_0$ to $1.09L_0$. On commensurate patterns ($L_s = L_0$), well-ordered assemblies were formed across the entire range of ϕ_H, as seen in previous studies on the assembly of cylindrical domains on commensurate chemical patterns.[12] When $L_s > L_0$, directed assembly of all of the blends yielded structures that displayed only a few defects. However, when $L_s < L_0$, and especially when $L_s = 0.9L_0$, the assembled films of pure PS-*b*-PMMA ($\phi_H = 0$) or of the ternary blend with $\phi_H = 0.1$ had a number of defects. In contrast, the ternary blends with $\phi_H = 0.2$ or 0.3 on patterns with $L_s < L_0$ had only a small number of defects.

The degree of order of the assembled arrays of cylinders presented in Figure 2 was quantified by determining OP_o of the SEM corresponding to each assembly. OP_o provides a measure of the angular distortion of the lattice points in the hexagonal unit cell. As seen in Figure 3, OP_o values were greater than 0.9 when the pure PS-*b*-PMMA or the ternary blends were assembled on chemical patterns with $L_s = L_0$. On the incommensurate chemical patterns with $L_s = 0.9L_0$, the OP_o values for the assemblies of blends with $\phi_H = 0.2$ or 0.3 were significantly higher than for the assemblies with $\phi_H = 0$ or 0.1. A similar result can be observed for the substrates with $L_s = 0.95L_0$. In effect, the addition of the

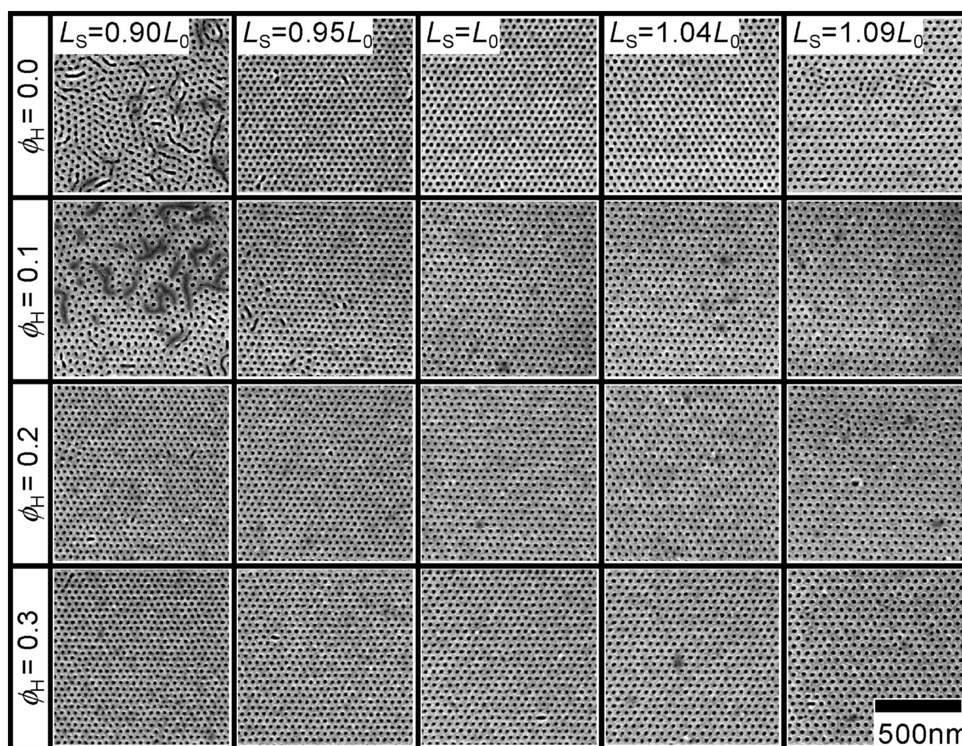

Figure 2. Top-down SEM images of thin films of PS-*b*-PMMA or PS-*b*-PMMA/PS/PMMA ternary blends directed to assemble on chemical patterns with various L_s. The volume fraction of homopolymers in the films is represented by ϕ_H.

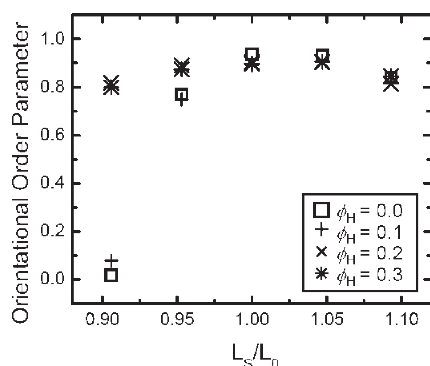

Figure 3. Combined effect of deviations from commensurability (expressed in terms of L_s/L_0) and homopolymer volume fraction (ϕ_H) on the orientational order parameter of the assembled cylindrical domains shown in Figure 2.

homopolymer to the PS-*b*-PMMA broadens the range of L_s over which well-ordered assemblies can be achieved.

Monte Carlo simulations were used to further analyze the assemblies shown in Figure 2. The simulations of the assembled block copolymer and ternary blend yielded similar structures, as well as variation with ϕ_H and L_s, as shown in Figure 4. In Figure 4, the blue and red regions are areas in which the normalized PMMA or PS density is close to 1.0, respectively. The PS–PMMA interface, which defines the surface of the cylindrical domains, has a normalized PMMA density close to 0.5 and is shown in yellow, both in the top-down and the three-dimensional cross section images. When $L_s = L_0$, the top-down images of the simulated assemblies showed highly ordered hexagonal arrays of domains. However, when ϕ_H = 0 or 0.1 and $L_s = 0.9L_0$, a number of defects were apparent in the assembly. As seen in the top-down images in Figure 4, the PS matrix, which was red when ϕ_H = 0, indicative of pure PS, became more orange as ϕ_H was increased, indicating that the matrix at the surface of the assembled film contained more PMMA.

While the top-down images of the simulations matched the experimental SEM results, the simulations offered additional information regarding the shape of the cylindrical domains. As seen in the cylinder sections on the right of Figure 4, the addition of homopolymer caused the cylinders to form with more of an hourglass shape. When ϕ_H = 0, the tops and bottoms of the cylinders were slightly larger than the center of the cylinder. However, as ϕ_H increased, the top and bottoms of the cylinders became significantly larger than the middle of the cylinder, and also they had a greater degree of variability from cylinder to cylinder compared to the cylinders in the ϕ_H = 0 case.

Density Multiplication of Ternary Blends on Chemical Patterns. After analyzing the effect of ϕ_H and L_s on the assembly of the cylinder-forming blends shown above, we investigated the effect that density multiplication would have on the assemblies. The results of directed assembly with 4:1 density multiplication of films of PS-*b*-PMMA and of ternary blends, with ϕ_H ranging from 0 to 0.3 on substrates with L_s ranging from $0.90L_0$ to $1.09L_0$, are presented in Figure 5. The pure PS-*b*-PMMA films assembled on the 4:1 chemical patterns with $L_s = L_0$

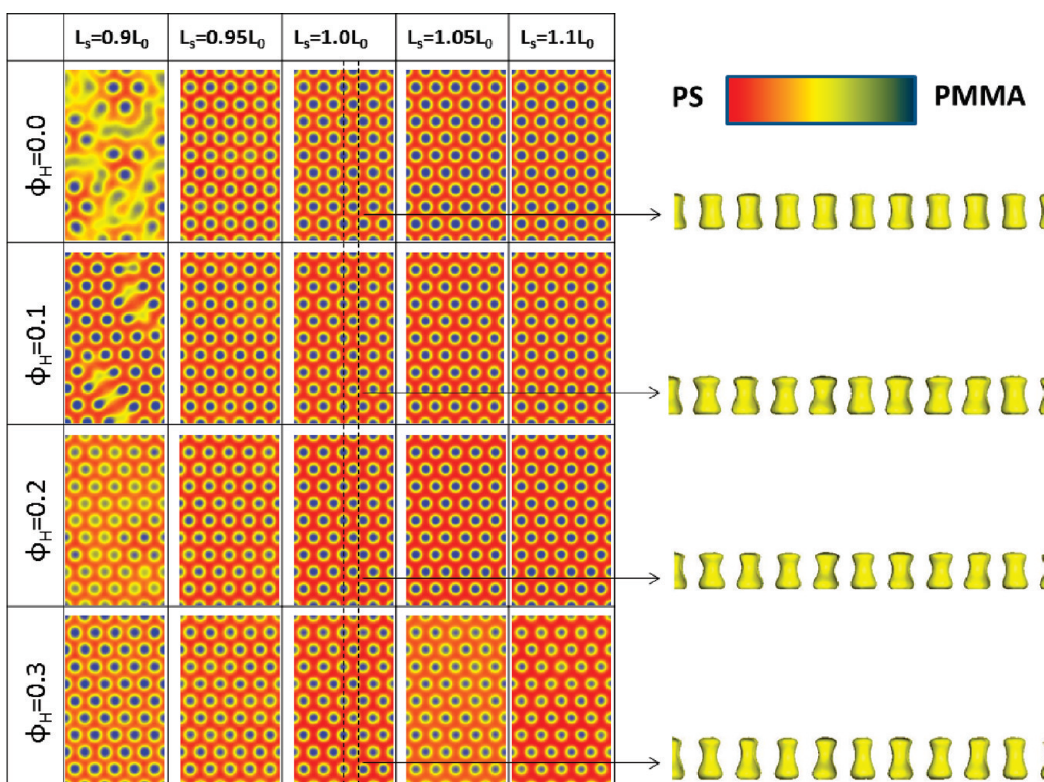

Figure 4. Top-down simulation images of 1:1 directed assembly of films of PS-*b*-PMMA or ternary blends on chemical patterns with various L_s, corresponding to the SEM images shown in Figure 2. The concentration of PS or PMMA in the structures is shown by the color scale bar in the upper right. The three-dimensional images on the right are representative samples of cylindrical domains taken from a section of the $L_s = L_0$ films, such as the section defined by the vertical dashed lines in the corresponding top-down image. The shape of the cylindrical domains became more like an hourglass as the fraction of homopolymer (ϕ_H) in the blends was increased from 0 to 0.3.

and $L_s = 1.04L_0$ with few defects and with only slightly less order than the corresponding assembly without density multiplication (Figure 2). Similar to the pure PS-*b*-PMMA, the best assemblies with the blends with $\phi_H = 0.1$ occurred on the substrates with $L_s = L_0$ and $L_s = 1.04L_0$. Good assemblies were also formed when $L_s = 0.90L_0$ and $\phi_H = 0$ or 0.1. For the blends with $\phi_H = 0.2$ or 0.3, the L_s window for the best assemblies shifted to lower values of L_s, with the best assemblies occurring at $L_s = 0.95L_0$ and $L_s = L_0$. Unlike the assemblies without density multiplication, the assemblies with density multiplication when $L_s = 0.9L_0$ showed no improvement in order as ϕ_H was increased from 0 to 0.3.

In general, the Monte Carlo simulations mirrored the experimentally observed structures, as shown in the top-down view of the simulated structures in Figure 6. There were some differences between the simulations and the SEMs, however. For example, the assembly of the pure PS-*b*-PMMA on chemical patterns with $L_s = 0.95L_0$ and $L_s = L_0$ exhibited a few defects, whereas the assemblies of the pure PS-*b*-PMMA on other chemical patterns did not. For the pure PS-*b*-PMMA, the best assemblies were achieved with $L_s = 1.05L_0$ and $L_s = 1.1L_0$. As ϕ_H was increased in the simulations, the window of L_s that yielded the best assemblies shifted to lower values of L_s, with the best assemblies for the blends with $\phi_H = 0.1$ occurring in the range of $L_s = L_0$ to $L_s = 1.1L_0$, the best assemblies for the blends with $\phi_H = 0.2$ occurring when $L_s = L_0$ or $L_s = 1.05L_0$, and the best assemblies for the blends with $\phi_H = 0.3$ occurring in the range of $L_s = 0.95L_0$ to $L_s = 1.05L_0$.

Monte Carlo simulations of the range of assemblies present in Figure 6 were again useful in providing insight into how the increase in ϕ_H affected the structure of the cylinders. Similar to the results of simulations of assemblies without density multiplication, the simulations suggested that the domains of pure PS-*b*-PMMA had a more uniform, cylindrical shape than the domains of the blends. As ϕ_H increased, the cylinders became increasingly more mis-shapen and tilted. In the case of $\phi_H = 0.3$, some of the cylinders appeared to have a toadstool shape, with one end large and the other small.

DISCUSSION

The results above provide insight into the combined effects of the assembled materials and the dimensions of the chemical pattern on the quality of the assembled morphology, as well as the shape of the assembled domains. First we analyze the effect of addition of homopolymer on the commensurability window, the range of L_s values that yields assemblies with well-ordered patterns. Then we examine the effect that the

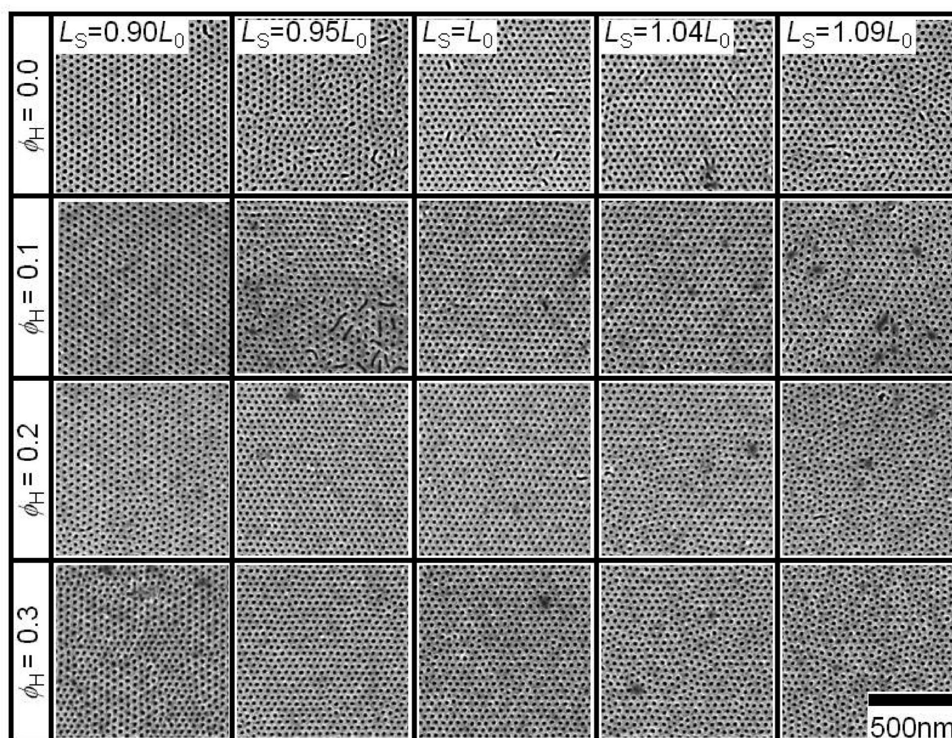

Figure 5. Top-down SEM images of thin films of PS-*b*-PMMA or PS-*b*-PMMA/PS/PMMA ternary blends directed to assemble on chemical patterns with 4:1 density multiplication. The effect of homopolymer volume fraction (ϕ_H) and change in pattern spacing (L_s) on the order of the assembled domains can be observed.

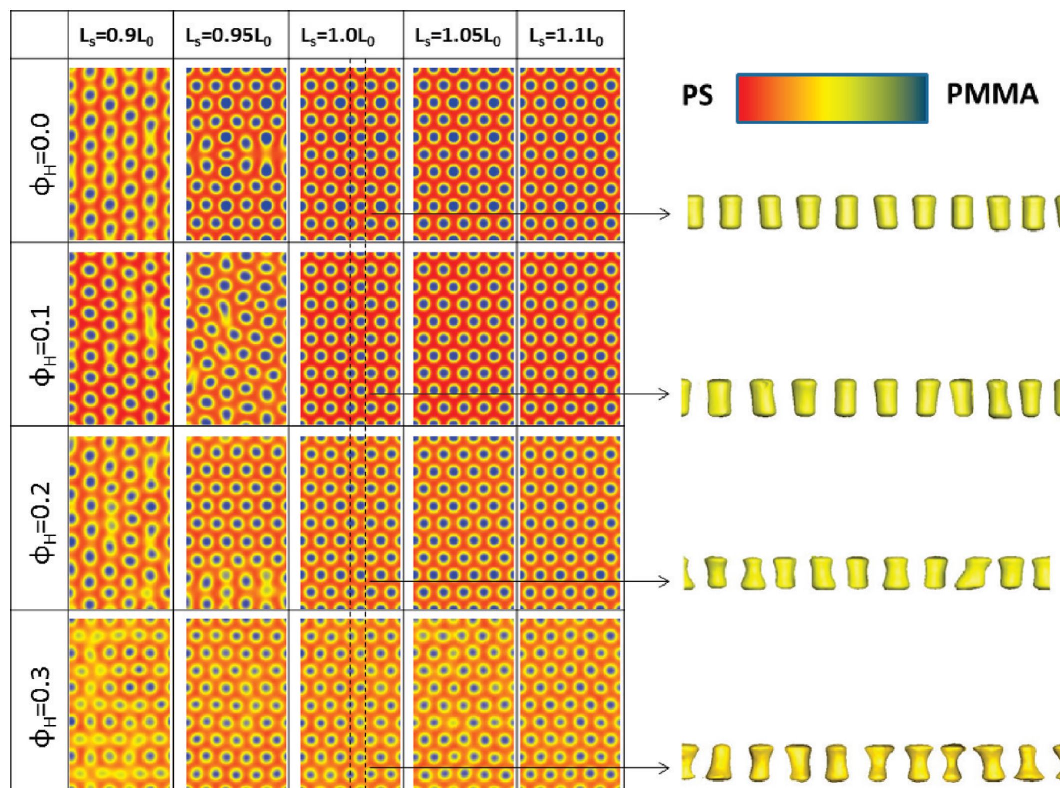

Figure 6. Top-down simulation images of thin films of PS-*b*-PMMA or PS-*b*-PMMA/PS/PMMA ternary blends directed to assemble on chemical patterns with 4:1 density multiplication, as a function of L_s and ϕ_H. The concentration of PS or PMMA in the structures is shown by the color scale bar in the upper right. The three-dimensional images of the cross section for $L_s = L_0$ show that the cylindrical domains became shaped more like an hourglass as the amount of homopolymer (ϕ_H) in the blends was increased from ϕ_H = 0 to 0.3.

addition of homopolymer had on the three-dimensional shape of the cylindrical domains. After analyzing the effect of homopolymer addition on the commensurability window and domain shape in the case of directed assembly without density multiplication, we repeat the analysis for directed assembly with density multiplication.

As shown in Figures 2 and 3, the addition of homopolymer led to a broadening of the commensurability window over which assemblies with high OP_o could be achieved. Instead of having a commensurability window of $\pm5\%$ (L_s relative to L_0) for pure block copolymer, the commensurability window could be increased to $\pm10\%$ by the addition of 20% homopolymer. However, the trade-off for the broadening of the commensurability was that the cylindrical domains became less uniform as ϕ_H increased, as seen in Figure 4.

In the case of the assemblies with density multiplication, careful inspection of the SEM images and the corresponding simulations (Figures 5 and 6) show that the commensurability window did not increase in size with increasing ϕ_H, as was the case for assemblies without density multiplication. In addition, the L_s values of the commensurability window shifted to smaller values with increasing ϕ_H. For example, in both Figures 5 and 6, the L_s values for the commensurability windows for $\phi_H = 0$ and 0.3 were L_0 to $1.04L_0$ and $0.95L_0$ to L_0, respectively. The shift in the window of L_s with ϕ_H can be understood in terms of the effect that the addition of homopolymer to a block copolymer has on the spacing of cylinders in the bulk. Block copolymer ternary blends with low M_n homopolymers have a tendency to have a smaller spacing between cylinders, L_b, than the corresponding cylinder spacing of the pure block copolymer, L_0, due to the even distribution of homopolymers within the cylindrical domains, which effectively decreases χ, the Flory–Huggins interaction parameter, at the domain–domain interface.[28–31] Previously, Stuen *et al.* studied the phase separation and the assembled morphology of cylinder-forming PS-*b*-PMMA/PS/PMMA ternary blends with respect to the molecular weights of homopolymers and ϕ_H and found that the addition of homopolymers with M_n values similar to those of the homopolymers used in this study could cause L_b of a blend with $\phi_H = 0.3$ to be almost 5% smaller than L_0.[25] Using the data of Stuen *et al.* to establish values of L_b for our blends, we can plot OP_o as a function of L_s/L_b of the assemblies done with density multiplication for each of the blends as well as the pure PS-*b*-PMMA, as shown in Figure 7 for the cases of 3:1 and 4:1 density multiplication. (Top-down SEMs used for determining the OP_o values for the 3:1 assemblies are shown in the Supporting Information.) For both cases, the curves for the three blends and the pure PS-*b*-PMMA overlapped fairly well and had the same window of L_s/L_b values that yielded assemblies with high OP_o. The curve for the blends with $\phi_H = 0.2$ appeared shifted to lower values of L_s/L_b, which could have been caused by

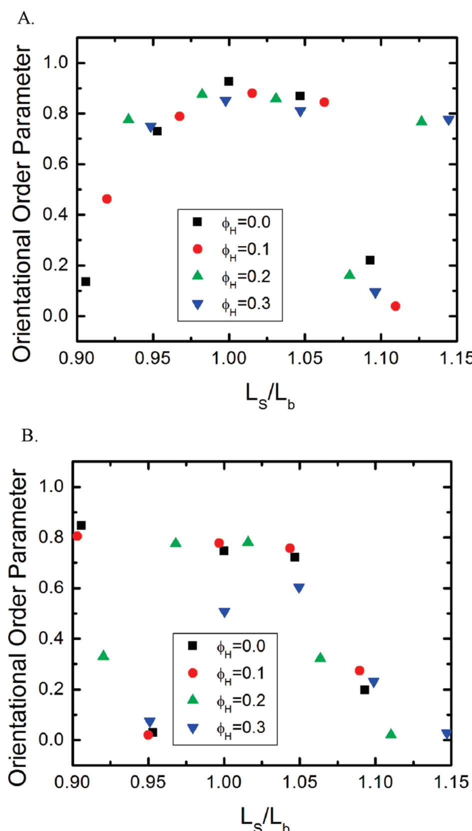

Figure 7. Orientational order parameter as a function of the ratio of chemical pattern spot spacing (L_s) to the cylinder spacing in the bulk of the blends (L_b) for ternary blend films assembled with a density multiplication factor of (A) 3:1 and (B) 4:1. The homopolymer volume fraction (ϕ_H) was varied from 0 (pure PS-*b*-PMMA) to 0.3, as shown in the legend.

variations in the data of Stuen *et al.*, but still matched the shape of the other three curves fairly well.

Other striking features of the graph shown in Figure 7 are the outlier points at $L_s/L_b > 1.1$ in Figure 7A and at $L_s/L_b \sim 0.9$ in Figure 7B. The high values of OP_o at $L_s/L_b \sim 0.9$ in Figure 7B reflect the high degree of order seen in the corresponding SEMs in Figure 5. These high values of OP_o at highly incommensurate values of L_s/L_b are due to the blends assembling with a different hexagonal orientation that enables a more commensurate fit of the assembled cylinders with the underlying spotted chemical pattern. As shown by Bita *et al.*, when hexagonal patterns are assembled within a sparse array of nodes, different orientations of the assembled hexagonal array can be achieved, depending on the spacing of the assembled array (L_b, in our case) and the spacing of the pattern (L_s).[32] When L_s is commensurate with L_b, the assembled hexagonal unit cell will orient with the same orientation as the sparse array of hexagonal nodes. However, as L_s diverges from commensurability with L_b, other orientations of the hexagonal unit cell can fit within the sparse array of nodes, such that there is effectively more commensurability between L_s and L_b. In our case, for an assembly with 3:1 density multiplication and $L_s/L_b \sim 1.15$, the

hexagon unit cell of the assembled cylinders can achieve better alignment with the underlying spots when it is rotated by 30° relative to the unit cell orientation when $L_s/L_b = 1$. Similarly, for an assembly with 4:1 density multiplication and $\phi_H = 0$, at $L_s/L_o \sim 0.9$, a rotation of the hexagon unit cell by 30° enables the cylinder spacing to be virtually commensurate with the spacing of the underlying spots, and as a result, a well-ordered assembly of cylinders is formed.

One of the ways in which the simulations are helpful in analyzing the assembled morphologies is that they can provide snapshots of the domains, as shown in Figures 4 and 6. A comparison of the 3D shapes of the domains obtained from the simulations reveals that, for pure block copolymer ($\phi_H = 0$), the domains in the 1:1 assembly had an hourglass shape, while the shape was more cylindrical for the 4:1 assembly. A similar effect is observed when comparing the domain shapes for blends with $\phi_H = 0.2$. In contrast, for blends with $\phi_H = 0.3$, it is difficult to discern whether or not the 4:1 assembly yielded more uniform domains than the 1:1 assembly.

When it is difficult to discern from the snapshot images a clear difference between the domains, it is useful to examine the average shape of the domains across an entire simulated assembly. One approach to examine the average domain shape is to use the simulation results to graph the density of PMMA chains, from both block copolymer and homopolymer, in successive layers parallel to the substrate. The average PMMA density (ρ_{PMMA}) across a layer of the entire simulation (corresponding to approximately cylindrical domains) at a given distance from the interface (expressed as z/L_0, where the film thickness in the simulation equaled L_0) scales with the diameter of the domain at that distance, such that the average density profile provides an idea of the average shape of the domain. The density profile close to the boundaries results from the assumption of $N = 32$ as described in our previous work.[33] This assumption effectively describes the behavior of the cylinders in this study while maintaining Gaussian statistics of the chains in the immediate vicinity of the wall.

Several trends are apparent in the PMMA density profile in Figure 8. First, for all of the assemblies, the density was lower at $z/L_0 = 0.5$ in comparison to $z/L_0 = 0.0$ and $z/L_0 = 1.0$, suggesting a larger domain diameter close to the chemical pattern interface and the surface of the film, in comparison to the middle, which corresponded to the hourglass shapes apparent in Figures 4 and 6. Second, for each value of ϕ_H, ρ_{PMMA}, and therefore the average diameter of the domain, was smaller for the assembly with 4:1 density multiplication compared to the assembly with 1:1 density multiplication. One possible reason for this difference could be that the domains that form between the patterned spots on the 4:1 chemical pattern did not wet the chemical pattern interface. In contrast, for each value of ϕ_H, ρ_{PMMA} was equal at

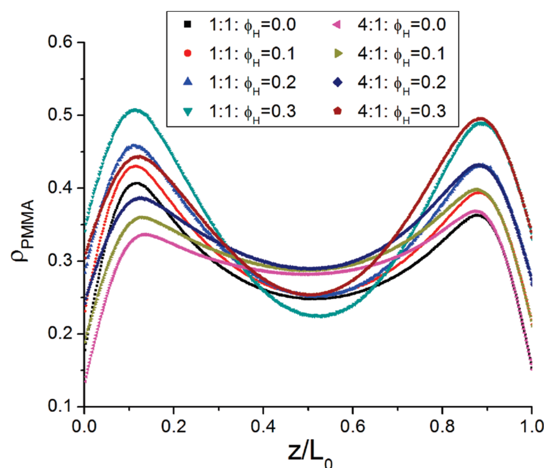

Figure 8. Average density of cylinder-forming polymer, ρ_{PMMA}, as a function of the ratio of film thickness (z) to the cylinder spacing in the bulk (L_0) with a density multiplication factor of 1:1 and 4:1. The results are plotted for four different homopolymer volume fractions (ϕ_H): 0 to 0.3.

the free surface of the film. Third, the comparison between the 1:1 and 4:1 assemblies at $\phi_H = 0.0$ suggests a smoother density profile and a smaller difference between the maximum and minimum values of ρ_{PMMA} for 4:1 assembly in comparison to 1:1. A similar trend can be seen for $\phi_H = 0.2$ and $\phi_H = 0.3$, although for $\phi_H = 0.3$, the difference in the minimum value of ρ_{PMMA} between the 1:1 and 4:1 assemblies is smaller than it is when $\phi_H = 0.2$. In general, the ρ_{PMMA} profile plots confirm that, for a given value of ϕ_H, the three-dimensional shapes for the 4:1 assembly are more cylindrical in comparison to 1:1 assembly.

In addition to the shapes of the PMMA cylinders, the density of the block copolymer chain ends (both PS and PMMA) was computed, in the same manner that ρ_{PMMA} was determined for Figure 8, to compare the mobility of the block copolymer chains for different assemblies. Figure 9 shows the film thickness along the x-axis and the average density of chain ends along the y-axis. The hourglass shapes that were observed in Figure 8 are also apparent in Figure 9. It should be noted that because the graph in Figure 9 represents the chain ends of only the block copolymer, the total density of chain ends of the blend ($\phi_H = 0.2$) will not be the same as the total density of chain ends of the pure block copolymer ($\phi_H = 0$). Also, the magnitude of the density values are small because the chain ends represent only 2 beads out of 30 that comprise the block copolymer in the simulation.

The hourglass shape of the domains can be understood as the combination of the varying chain mobility of the different blends and the thermodynamic driving force for wetting of the chemical pattern by the PMMA. The patterned spots had an affinity for PMMA set by $\Lambda N = 1$, whereas the affinity for PS by the background region was $\Lambda N = 0.15$. Thus, there was a greater affinity for PMMA to be near the spots than for PS to be near the surrounding background region. In the case of the

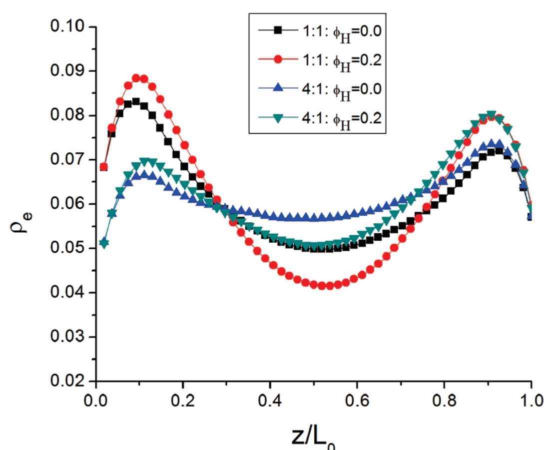

Figure 9. Average density of chain ends of diblock as a function of the ratio of film thickness (z) to the cylinder spacing in the bulk (L_0) with a density multiplication factor of 1:1 and 4:1. The homopolymer volume fraction (ϕ_H) shown was 0 (pure PS-*b*-PMMA) and 0.2.

films assembled with density multiplication, there were fewer patterned spots and therefore fewer places where the PMMA extended all the way to the chemical pattern. Thus, the 1:1 assemblies will have more PMMA at small values of z/L_0 (near the chemical pattern) than the 4:1 assemblies. This difference is most apparent when comparing the 1:1 and 4:1 assemblies in Figure 9. Because more of the PMMA (Figure 8) and chain ends (Figure 9) are at the chemical pattern interface in the 1:1 assemblies when compared to the 4:1 assemblies, there will be less PMMA, or fewer chain ends, at the middle of the film, and therefore the hourglass shape is more pronounced. We would also expect the polymers in the blend to have more mobility than pure block copolymer. This increased mobility of the blend appears to cause a more pronounced hourglass shape when compared to the corresponding assembly for pure block copolymer. Both the thermodynamic and mobility effects are important to consider for technological applications. The decrease in the hourglass structure with density multiplication can provide greater uniformity of pattern features and decreased line edge roughness, while the increase in chain mobility may lead to an increase in hourglass shape, but also improved annealing, and therefore structures with fewer defects.

We can use the combined experimental and simulation results to consider the technological implications for the use of directed assembly in bit patterned media. First, in the case of 1:1 directed assembly, the addition of homopolymer can increase the commensurability window from $\pm5\%$ of L_s to $\pm10\%$ of L_s, which is beyond the requirements for bit patterned media for the variation in spot spacing. However, in the case of 1:1 directed assembly, a question remains regarding whether the domains are sufficiently uniform in three-dimensional shape to yield uniform spots after transfer of the assembled pattern to the underlying substrate. Pattern transfer itself depends on many variables (transfer method, etch conditions, *etc.*), but one feature that directed assembly without density multiplication has working in its favor is that each cylindrical domain will wet a spot on the chemical pattern. Those spots should have approximately the same area, within the limits of the lithographic process used to pattern them. The uniformity of these spots at the block copolymer/chemical pattern interface suggests that, with the proper pattern transfer method, the assembled cylinders could be sufficient for pattern transfer for bit patterned media. The results also show that the trade-offs between commensurability window and domain shape are the opposite when the assemblies are performed with density multiplication. For the assemblies with density multiplication, the commensurability window does not increase beyond $\pm5\%$ of L_s, but when compared to 1:1 assemblies, the average shape of the domains is more cylindrical.

CONCLUSION

Our work reveals the trade-offs inherent in adding homopolymer to a cylinder-forming block copolymer to be used for directed assembly, both with and without density multiplication. In the case of directed assembly without density multiplication, the use of a blend instead of pure block copolymer can increase the range of domain spacings over which the blend can be assembled with a high degree of order, but that the resulting cylindrical domains of the blend will not be as uniform as they are for the pure block copolymer. In contrast, directed assembly with density multiplication of the blend leads to a more uniform domain shape than without density multiplication, but the range of domain spacings achievable with the assembly of the blend does not improve compared to the range achievable with 1:1 directed assembly of the pure block copolymer. The results of this work should point the way for the implementation of directed assembly of cylinder-forming block copolymer with density multiplication in technologies such as advanced lithography and bit patterned media.

EXPERIMENTAL AND SIMULATION SECTION

Materials. Cylinder-forming PS-*b*-PMMA (M_n = 50.5 kg/mol PS and 20.9 kg/mol PMMA, and PDI = 1.06, bulk center-to-center distance between cylinders (L_0) ≈ 43 nm), PS (M_n = 1.5 kg/mol and PDI = 1.05), and PMMA (M_n = 1.5 kg/mol and PDI = 1.06) were acquired from Polymer Source, Inc. and used as received. The homopolymers were added to the blend in a PS/PMMA ratio of 73:27 (v/v) to match the volume fractions of the PS-*b*-PMMA. The homopolymer fraction in the ternary blends (ϕ_H) was varied from 0 to 0.3. Hydroxyl-terminated polystyrene

ARTICLE

(PS−OH; M_n = 6.0 kg/mol, PDI = 1.07) was synthesized using anionic polymerization. PMMA photoresist was purchased from MicroChem Corp. and had a M_n of 950 kg/mol.

Preparation of Chemically Patterned Surfaces. Chemical patterns were prepared from the PS−OH brush to yield a hexagonal array of spots, with the center-to-center distance between spots on the pattern (L_s) ranging from $0.9L_0$ to $1.1L_0$. The spots were preferentially wet by the PMMA block of the PS-*b*-PMMA, and the matrix surrounding the spots was preferentially wet by the PS block. Generating patterns for directed assembly with density multiplication was achieved by selectively removing spots from the hexagonal array, such that the density of cylindrical domains of the assembled block copolymer was an integer multiple of the surface density of spots in the chemical pattern. Chemical patterns were generated for density multiplication factors ranging from 1:1 to 4:1.

The process to form the chemical pattern started with spin-coating a ∼20 nm thick film of PS−OH onto a piranha-cleaned silicon wafer from a 1.0 wt % toluene solution. The PS−OH film was annealed under vacuum at ∼160 °C for 2 days in order to graft the PS−OH to the wafer *via* a dehydration reaction. Ungrafted PS−OH was then extracted using repeated sonications in warm toluene for no more than 10 min, resulting in a brush-coated wafer, as explained previously.[23,34] The grafted PS−OH was patterned in a manner similar to the method suggested by Stoykovich *et al.*[34] A 50 nm thick PMMA photoresist film was spin-coated from a chlorobenzene solution on top of a brush-coated substrate. Electron-beam lithography was performed using a LEO 1550-VP field emission scanning electron microscope (SEM) operating with a J.C. Nabity nanoscale pattern generation system. Exposures utilized an accelerating voltage of 20 keV, a beam current of ∼27.5 pA, and line doses in the range of 0.08−0.60 nC/cm. All samples were developed for 30 s in a 1:3 solution of methyl isobutyl ketone/isopropyl alcohol, followed by IPA rinsing and nitrogen drying steps. Subsequently, the photoresist pattern was transferred to a chemical pattern in the PS brush by oxygen plasma etching, using a PE-200 Benchtop Plasma System (Plasma Etch, Inc.) plasma etch device, operated at 10 mTorr pressure, an O_2 flow rate of 10 sccm, and a radio frequency power of 80 W for 10 s. The oxygen-plasma-treated regions of the brush were preferentially wet by PMMA, and the untreated PS−OH regions were preferentially wet by the PS.

Assembly. The polymeric materials were spin-coated from 1.3% solutions in toluene onto the chemically patterned surfaces. The resulting block copolymer thin film was 37 nm thick, as measured by ellipsometry (Rudolph Research Auto EL). The film was annealed under vacuum at 230 °C for 6 h.

Characterization and Analysis. The patterns and the domain structures of the assembled block copolymer films on the chemical nanopatterns were imaged using a LEO 1550-VP field emission SEM with 1 keV acceleration voltage. To assist in image contrast for the films, the PMMA portions of the film were removed with 0.5 J/cm^2 exposures of 254 nm ultraviolet light followed by a 30 s rinse in glacial acetic acid, subsequent washing with deionized water, and drying by nitrogen gun. The orientational order parameter (OP_o) of hexagonally ordered cylinders of annealed block copolymer films on the various chemical patterns was determined by a custom MATLAB program after normalizing the brightness and contrast of the images with Photoshop.[26] The OP_o was determined from a hexagonal lattice point and its six nearest neighbors in our case. The data presented for each condition were collected from more than 2000 cylinders per sample.

Monte Carlo Simulations. Monte Carlo (MC) simulations were performed for 10^5 cycles using a coarse-grained model to describe block copolymer melts.[27] To discretize each chain contour, N beads were used, and the chains of the block copolymer were confined in a volume V at temperature T.[35] The two energy components of the Hamiltonian H were the bonded component (H_b), described by pairwise interaction function between beads, and the nonbonded component (H_{nb}), described by a function of the local densities $\Phi_A(r)$ and $\Phi_B(r)$.[36] The bonded interactions correspond to the harmonic springs of the Gaussian chains:

$$\frac{H_b[r_i(s)]}{k_BT} = \frac{3}{2}\sum_{s=1}^{N-1}\frac{[r_i(s+1) - r_i(s)]^2}{b^2} \tag{1}$$

where vector $r_i(s)$ denotes the position of the sth bead in the ith chain, $b^2 = R_e^2/(N-1)$ is the mean squared bond length, k_B is the Boltzmann constant, and R_e is the mean squared end-to-end distance for an isolated, non-interacting chain. For nonbonded interactions, the densities were computed from the bead positions, giving rise to a pairwise interaction potential. The simple form of nonbonded interactions is

$$\frac{H_{nb}[\Phi_A, \Phi_B]}{k_BT} = \rho_0\int_V dr\left[\chi\Phi_A\Phi_B + \frac{\kappa}{2}(1 - \Phi_A - \Phi_B)^2\right] \tag{2}$$

where Flory−Huggins parameter is χ and ρ_0 is the average bulk number density of beads. The local density fluctuations were restricted to deviate from the average value of eq 2 obtained by the finite compressibility, where κ is related to the inverse isothermal compressibility of the melt. The invariant degree of polymerization $\bar{N}$ is proportional to M_n for this dense melt. The length scale used in our model was the coarse grain parameter R_e and was set by $\sqrt{\bar{N}} = \rho_0 R_e^3/N$. The $\sqrt{\bar{N}}$ parameter was used to estimate the number of chains a given chain interacts with, which in turn controls the strength of the fluctuations. For our simulations of a cylinder-forming AB diblock copolymer, we used $\chi N = 25$, $\kappa N = 35$, $\bar{N} = 95^2$, which corresponded to a diblock copolymer with M_n = 71.4 kg·mol^{-1} and approximately matched the PS-*b*-PMMA used in our experiments. The diblock copolymer chain (with N = 30 beads) was discretized into N_A = 21 and N_B = 9 beads, respectively, corresponding to each block of the diblock and will be referred to as block A and B. Homopolymers of A and B are represented by a single bead each. The thickness of the thin film in the simulation was similar to those of experiments, and the simulation results were rescaled such that the thickness equaled L_0. To represent the chemical pattern of the surface, we used the potential given by[37,38]

$$\frac{U(r, K)}{k_BT} = -\frac{\Lambda^K}{d/R_e}\exp\left[-\frac{z^2}{2d^2}\right] \tag{3}$$

where $d = 0.15\ R_e$ and $\Lambda^K N$ sets the affinity between the surface and beads of type K. The top surface was neutral ($\Lambda N = 0$), and the patterned area on the bottom surface had a strong preference to the minority component ($\Lambda N = 1$). The unpatterned surface was slightly attractive to the majority block ($\Lambda N = -0.15$), and it was assumed that for all surfaces S, $\Lambda_S^A N = -\Lambda_S^B N = \Lambda_S N$. The surface term is added to the Hamiltonian $H = H_b + H_{nb} + H_S$, where $H_S = \sum_i U_S(r_i,K_i)$, which sums over all beads i, and U_S includes the potential.

Acknowledgment. This work was supported by the Semiconductor Research Corporation (SRC) and the National Science Foundation through the Nanoscale Science and Engineering Center (DMR-0425880). This work was based upon research conducted at the Synchrotron Radiation Center, University of Wisconsin—Madison, which is supported by the NSF under Award DMR-0537588.

Supporting Information Available: Top-down SEM images of thin films of PS-*b*-PMMA or PS-*b*-PMMA/PS/PMMA ternary blends directed to assemble on chemical patterns with 3:1 density multiplication are shown. The effect of homopolymer volume fraction (ϕ_H) and change in pattern spacing (L_s) on the order of the assembled domains can be observed. This material is available free of charge *via* the Internet at http://pubs.acs.org.

REFERENCES AND NOTES

1. Black, C. Block Copolymers: Nanowire Arrays Build Themselves. *Nat. Nanotechnol.* **2007**, *2*, 464–465.
2. Black, C.; Guarini, K.; Breyta, G.; Colburn, M.; Ruiz, R.; Sandstrom, R.; Sikorski, E.; Zhang, Y. Highly Porous Silicon Membrane Fabrication Using Polymer Self-Assembly. *J. Vac. Sci. Technol., B* **2006**, *24*, 3188.
3. Black, C.; Ruiz, R.; Breyta, G.; Cheng, J.; Colburn, M.; Guarini, K.; Kim, H. C.; Zhang, Y. Polymer Self Assembly in Semiconductor Microelectronics. *IBM J. Res. Dev.* **2010**, *51*, 605–633.
4. Cheng, J. Y.; Ross, C. A.; Chan, V. Z. H.; Thomas, E. L.; Lammertink, R. G. H.; Vancso, G. J. Formation of a Cobalt

Magnetic Dot Array *via* Block Copolymer Lithography. *Adv. Mater.* **2001**, *13*, 1174–1178.
5. Cheng, J.; Ross, C.; Thomas, E.; Smith, H. I.; Vancso, G. Fabrication of Nanostructures with Long-Range Order Using Block Copolymer Lithography. *Appl. Phys. Lett.* **2002**, *81*, 3657.
6. Kim, S. H.; Misner, M. J.; Xu, T.; Kimura, M.; Russell, T. P. Highly Oriented and Ordered Arrays from Block Copolymers *via* Solvent Evaporation. *Adv. Mater.* **2004**, *16*, 226–231.
7. Park, M.; Harrison, C.; Chaikin, P. M.; Register, R. A.; Adamson, D. H. Block Copolymer Lithography: Periodic Arrays of Similar to 10(11) Holes in 1 Square Centimeter. *Science* **1997**, *276*, 1401–1404.
8. Ruiz, R.; Ruiz, N.; Zhang, Y.; Sandstrom, R. L.; Black, C. T. Local Defectivity Control of 2D Self Assembled Block Copolymer Patterns. *Adv. Mater.* **2007**, *19*, 2157–2162.
9. Segalman, R. A.; Yokoyama, H.; Kramer, E. J. Graphoepitaxy of Spherical Domain Block Copolymer Films. *Adv. Mater.* **2001**, *13*, 1152–1155.
10. Thurn-Albrecht, T.; Schotter, J.; Kastle, G.; Emley, N.; Shibauchi, T.; Krusin-Elbaum, L.; Guarini, K.; Black, C.; Tuominen, M.; Russell, T. Ultrahigh-Density Nanowire Arrays Grown in Self-Assembled Diblock Copolymer Templates. *Science* **2000**, *290*, 2126.
11. Wang, Q.; Nealey, P. F.; de Pablo, J. J. Simulations of the Morphology of Cylinder-Forming Asymmetric Diblock Copolymer Thin Films on Nanopatterned Substrates. *Macromolecules* **2003**, *36*, 1731–1740.
12. Park, S. M.; Craig, G. S. W.; Liu, C. C.; La, Y. H.; Ferrier, N. J.; Nealey, P. F. Characterization of Cylinder-Forming Block Copolymers Directed To Assemble on Spotted Chemical Patterns. *Macromolecules* **2008**, *41*, 9118–9123.
13. Han, E.; Stuen, K. O.; La, Y. H.; Nealey, P. F.; Gopalan, P. Effect of Composition of Substrate-Modifying Random Copolymers on the Orientation of Symmetric and Asymmetric Diblock Copolymer Domains. *Macromolecules* **2008**, *41*, 9090–9097.
14. Ruiz, R.; Kang, H.; Detcheverry, F. A.; Dobisz, E.; Kercher, D. S.; Albrecht, T. R.; de Pablo, J. J.; Nealey, P. F. Density Multiplication and Improved Lithography by Directed Block Copolymer Assembly. *Science* **2008**, *321*, 936–939.
15. Kang, H. M.; Stuen, K. O.; Nealey, P. F. Directed Assembly of Cylinder-Forming Ternary Blend of Block Copolymer and Their Respective Homopolymers on Chemical Patterns with Density Multiplication of Features. *J. Photopolym. Sci. Technol.* **2010**, *23*, 297–299.
16. Kang, H. M.; Detcheverry, F.; Stuen, K. O.; Craig, G. S. W.; de Pablo, J. J.; Gopalan, P.; Nealey, P. F. Shape Control and Density Multiplication of Cylinder-Forming Ternary Block Copolymer−Homopolymer Blend Thin Films on Chemical Patterns. *J. Vac. Sci. Technol., B* **2010**, *28*, C6B24–C6B29.
17. Ruiz, R.; Dobisz, E.; Albrecht, T. R. Rectangular Patterns Using Block Copolymer Directed Assembly for High Bit Aspect Ratio Patterned Media. *ACS Nano* **2011**, *5*, 79–84.
18. Xiao, S.; Yang, X.; Park, S.; Weller, D.; Russell, T. P. A Novel Approach to Addressable 4 teradot/in.^{2} Patterned Media. *Adv. Mater.* **2009**, *21*, 2516–2519.
19. Xiao, S. G.; Yang, X. M.; Edwards, E. W.; La, Y. H.; Nealey, P. F. Graphoepitaxy of Cylinder-Forming Block Copolymers for Use as Templates To Pattern Magnetic Metal Dot Arrays. *Nanotechnology* **2005**, *16*, S324–S329.
20. Dobisz, E. A.; Bandic, Z. Z.; Wu, T. W.; Albrecht, T. Patterned Media: Nanofabrication Challenges of Future Disk Drives. *Proc. IEEE* **2008**, *96*, 1836–1846.
21. Kim, S. O.; Solak, H. H.; Stoykovich, M. P.; Ferrier, N. J.; de Pablo, J. J.; Nealey, P. F. Epitaxial Self-Assembly of Block Copolymers on Lithographically Defined Nanopatterned Substrates. *Nature* **2003**, *424*, 411–414.
22. Rockford, L.; Liu, Y.; Mansky, P.; Russell, T. P.; Yoon, M.; Mochrie, S. G. J. Polymers on Nanoperiodic, Heterogeneous Surfaces. *Phys. Rev. Lett.* **1999**, *82*, 2602–2605.
23. Edwards, E. W.; Montague, M. F.; Solak, H. H.; Hawker, C. J.; Nealey, P. F. Precise Control over Molecular Dimensions of Block-Copolymer Domains Using the Interfacial Energy of Chemically Nanopatterned Substrates. *Adv. Mater.* **2004**, *16*, 1315–1319.
24. Park, S. M.; Stoykovich, M. P.; Ruiz, R.; Zhang, Z.; Black, C. T.; Nealey, P. F. Directed Assembly of Lamellae-Forming Block Copolymers Using Chemically and Topographically Patterned Substrates. *Adv. Mater.* **2007**, *19*, 607.
25. Stuen, K. O.; Thomas, C. S.; Liu, G. L.; Ferrier, N.; Nealey, P. F. Dimensional Scaling of Cylinders in Thin Films of Block Copolymer−Homopolymer Ternary Blends. *Macromolecules* **2009**, *42*, 5139–5145.
26. Liu, C. C.; Craig, G. S. W.; Kang, H. M.; Ruiz, R.; Nealey, P. F.; Ferrier, N. J. Practical Implementation of Order Parameter Calculation for Directed Assembly of Block Copolymer Thin Films. *J. Polym. Sci., Part B: Polym. Phys.* **2010**, *48*, 2589–2603.
27. Detcheverry, F. A.; Pike, D. Q.; Nagpal, U.; Nealey, P. F.; de Pablo, J. J. Theoretically Informed Coarse Grain Simulations of Block Copolymer Melts: Method and Applications. *Soft Matter* **2009**, *5*, 4858–4865.
28. Matsen, M. W. Phase-Behavior of Block-Copolymer Homopolymer Blends. *Macromolecules* **1995**, *28*, 5765–5773.
29. Winey, K. I.; Thomas, E. L.; Fetters, L. J. Swelling a Lamellar Diblock Copolymer with Homopolymer—Influences of Homopolymer Concentration and Molecular-Weight. *Macromolecules* **1991**, *24*, 6182–6188.
30. Dai, K. H.; Kramer, E. J.; Shull, K. R. Interfacial Segregation in 2-Phase Polymer Blends with Diblock Copolymer Additives—The Effect of Homopolymer Molecular-Weight. *Macromolecules* **1992**, *25*, 220–225.
31. Komura, S.; Kodama, H.; Tamura, K. Real-Space Mean-Field Approach to Polymeric Ternary Systems. *J. Chem. Phys.* **2002**, *117*, 9903–9919.
32. Bita, I.; Yang, J. K. W.; Jung, Y. S.; Ross, C. A.; Thomas, E. L.; Berggren, K. K. Graphoepitaxy of Self-Assembled Block Copolymers on Two-Dimensional Periodic Patterned Templates. *Science* **2008**, *321*, 939–943.
33. Detcheverry, F. A.; Kang, H. M.; Daoulas, K. C.; Muller, M.; Nealey, P. F.; de Pablo, J. J. Monte Carlo Simulations of a Coarse Grain Model for Block Copolymers and Nanocomposites. *Macromolecules* **2008**, *41*, 4989–5001.
34. Stoykovich, M. P.; Muller, M.; Kim, S. O.; Solak, H. H.; Edwards, E. W.; de Pablo, J. J.; Nealey, P. F. Directed Assembly of Block Copolymer Blends into Nonregular Device-Oriented Structures. *Science* **2005**, *308*, 1442–1446.
35. Daoulas, K. C.; Muller, M.; de Pablo, J. J.; Nealey, P. F.; Smith, G. D. Morphology of Multi-Component Polymer Systems: Single Chain in Mean Field Simulation Studies. *Soft Matter* **2006**, *2*, 573–583.
36. Daoulas, K. C.; Müller, M. Single Chain in Mean Field Simulations: Quasi-Instantaneous Field Approximation and Quantitative Comparison with Monte Carlo Simulations. *J. Chem. Phys.* **2006**, *125*, 184904.
37. Kang, H.; Detcheverry, F.; Stuen, K. O.; Craig, G. S. W.; de Pablo, J. J.; Gopalan, P.; Nealey, P. F. Shape Control and Density Multiplication of Cylinder-Forming Ternary Block Copolymer−Homopolymer Blend Thin Films on Chemical Patterns. *J. Vac. Sci. Technol., B* **2010**, *28*, C6B24–C6B29.
38. Detcheverry, F.; Liu, G.; Nealey, P.; de Pablo, J. Interpolation in the Directed Assembly of Block Copolymers on Nanopatterned Substrates: Simulation and Experiments. *Macromolecules* **2010**, *43*, 3446–3454.